Journal of Photochemistry and Photobiology A: Chemistry 256 (2013) 7–15

Contents lists available at SciVerse ScienceDirect

Journal of Photochemistry and Photobiology A: Chemistry

journal homepage: www.elsevier.com/locate/jphotochem

Enhanced photocatalytic degradation of dyes by TiO_2 nanobelts with hierarchical structures

A. Hu[a,*], R. Liang[a], X. Zhang[b], S. Kurdi[a], D. Luong[b], H. Huang[a], P. Peng[a], E. Marzbanrad[a], K.D. Oakes[b], Y. Zhou[a], M.R. Servos[b,**]

[a] Department of Mechanical and Mechatronics Engineering, University of Waterloo, 200 University Avenue West, Waterloo, Ontario, Canada
[b] Department of Biology, University of Waterloo, 200 University Avenue West, Waterloo, Ontario, Canada

ARTICLE INFO

Article history:
Received 17 October 2012
Received in revised form 11 January 2013
Accepted 31 January 2013
Available online 19 February 2013

Keywords:
TiO_2 nanowires
Hierarchical structure
Surface adsorption
Photocatalytic degradation

ABSTRACT

TiO_2 nanobelt membranes with hierarchical structure were successfully synthesized by sequentially autoclaving Ti at 190 °C for 3 d in the presence of 10 M NaOH and 10 M KOH solutions. Microstructural characterization revealed TiO_2 nanoparticles joining together and on the surface of nanobelts. These hierarchical structures form a three dimensional porous membrane which significantly enhances both surface specific area and light absorption, resulting in improved chemical adsorption capacity and photocatalytic degradation efficiency relative to nanobelts with smooth surfaces using methylene blue as a model molecule. The adsorption of methylene blue to these structures follows a pseudo-second order kinetics chemisorption mechanism with rate-limited diffusion correlated to pore structure and size. The dominant reactive oxygen species are identified as hydroxyl radicals and valence band holes through the scavenging reaction. The synergistic enhancement of filtration through surface adsorption and photocatalytic degradation is also demonstrated in a prototype photocatalytic membrane reactor with UV excitation at 365 nm. The reuse of nanobelt membranes after annealing shows the excellent recovery of TiO_2 catalyst. These studies may contribute to additional applications of hierarchical TiO_2 nanobelt membranes, including those harnessing sunlight for water treatment.

1. Introduction

The dominant causes of surface water and groundwater pollution are industrial discharges, landfill leachates, agricultural runoff, and municipal wastewater effluents which contain a myriad of contaminants including nutrients, pesticides as well as pharmaceuticals and personal care products (PPCPs) [1–3]. Conventional wastewater treatment utilizes various mechanical, chemical, biological and/or physical processes. Wastewater treatment plants (WWTPs) frequently combine multiple processes in their operations, such as coagulation–flocculation–sedimentation, biological degradation, filtration, chlorination, and ozonation during water treatment. Many of these methods require high operating/maintenance costs or, in the case of chlorination, release disinfection by-products or produce unintended consequences in receiving environment fauna [4]. Biological treatment, while inexpensive, cannot degrade many toxic or bio-recalcitrant organic compounds, such as pharmaceuticals or dyes [5–7]. Dyes are environmentally-relevant contaminants found in wastewater from textile, printing and paper manufacturing industries. The need for economically-feasible approaches to remove these waterborne contaminants promoted the development of innovative water treatment technologies.

Many environmental remediation techniques employ simple physical processes such as adsorption to effectively remove non-biodegradable, environmentally hazardous substances. Activated carbon and a suite of other low-cost, high-sorbing materials such as biomass, agricultural and industrial solid waste, clays and zeolites have been extensively investigated as alternative adsorbents for color removal [8,9]. Conversely, advanced oxidation processes (AOPs) are increasingly applied as an energy intensive but highly effective means of non-selectively degrading various organic pollutants including PPCPs and dyes. AOPs rely upon the generation of highly reactive short-lived transitory species (principally hydroxyl radicals), to efficiently degraded or even mineralize a wide range of organics into smaller biodegradable compounds or inorganic molecules like CO_2 and H_2O [10,11]. Some AOPs employ wideband semiconductive catalysts such as TiO_2, ZnO, Fe_2O_3, SnO_2, WO_3, and CdS. TiO_2 in particular has attracted considerable research attention as a non-toxic, chemically inert and photostable catalyst capable of degrading waterborne dyes among other pollutants. TiO_2 nanoparticles have been successfully applied within prototype WWTPs

* Corresponding author. Tel.: +1 519 8884567 35464.
** Corresponding author.
E-mail addresses: a2hu@uwaterloo.ca, anminghu@bjut.edu.cn (A. Hu), mservos@uwaterloo.ca (M.R. Servos).

1010-6030/$ – see front matter © 2013 Elsevier B.V. All rights reserved.
http://dx.doi.org/10.1016/j.jphotochem.2013.01.015

including those focussed on dye decoloration applications [5]. Two photocatalyst loading methods have been investigated: TiO_2 nanoparticle slurries and immobilized TiO_2 nanoparticles embedded on a reaction surface. TiO_2 nanoparticle slurries are a highly efficient means of treating water by photocatalytic degradation as the nanoparticles mix well with waterborne contaminants and allow for relatively unimpeded light exposure [1]. However, TiO_2 nanoparticles must subsequently be separated from the treated water, which represents a logistically challenging and energetically costly step [1,12]. Recently, TiO_2 nanowire/nanotube membranes have been developed as a multifunctional material for water treatment, which promises to combine three removal mechanisms: surface adsorption [9], ultrafiltration [11–13] and photocatalytic degradation [11,12,14]. However, the adsorption kinetics of TiO_2 nanowire membranes have not been systematically established. Contaminant degradation by TiO_2 nanowire membranes used as catalysts in photocatalytic membrane reactors (PMRs) may benefit from synergies arising from combinations of two or three removal mechanisms; to date, the potential of such synergistic interactions has not been explored.

Photocatalytic efficiency can be influenced by many physical and chemical features of catalysts, such as large and highly reactive surface areas, enhanced light adsorption, and the suppressed recombination of photo-generated electrons and holes [15–17]. Specially-designed nanowires with structural hierarchy can effectively suppress electron–hole recombination and improve photocatalytic efficiency. Mixtures of anatase and rutile phase TiO_2 nanoparticles (in 4:1 ratios; P25, Degassa) display a high photocatalytic efficiency [18] as does a TiO_2(B) nanowire with an anatase shell [19]. Fu et al. found that dispersived Au nanoparticles on TiO_2 films is also effectively improved the photocatalytic efficiency [20]. Liu et al. reported another highly efficient heterogeneous nanostructure in which anatase nanoparticles are layer-by-layer assembled on rutile nanorods [21]. Recently, Zhou et al. [17] synthesized long TiO_2 nanobelts embedded with surface anatase nanoparticles using the acid hydrothermal method. Charge transfers between nanobelts and nanoparticles leads to dramatically improved charged pair separation. From an engineering perspective, simple methods for synthesizing TiO_2 nanowire membranes with heterostructures in scalable volumes would significantly facilitate adoption of these materials in numerous applications.

In this work, we developed a facile method of fabricating TiO_2 membranes with structural hierarchy, in which TiO_2 nanoparticles can be grown on the surface of nanobelts. These hierarchical structures demonstrated enhanced surface adsorption and photocatalytic degradation efficiencies towards the dye methylene blue. A prototype photocatalytic membrane reactor was designed and tested with the newly developed TiO_2 nanobelt membranes, where the synergistic degradation of methylene blue by both surface adsorption and photocatalytic degradation was confirmed.

2. Experimental procedure

2.1. Chemicals and materials

Unless otherwise specified, all reagents and chemicals were of analytical grade and purchased from Sigma–Aldrich. TiO_2 nanobelts were synthesized using modified hydrothermal growth techniques. TiO_2 anatase nanobelts were grown for 48 h in 10 M NaOH solution within 125 mL Teflon®-lined acidic digestion reactors (Parr Instruments) at 190 °C using Ti foil as the titanium source and a small amount of carboxyl solvents as oxygen source [11,22]. Subsequently, the suspension nanobelts were separated from the NaOH solution by centrifugation, potentially generating 2 g of nanobelt within 60 mL of solution. The fabricated nanobelts were then dispersed into 10 M KOH solution and grown for another 24 h at 190 °C. Following the KOH autoclaving, nanobelts were again centrifugally separated and washed in 0.1 M HCl solution and deionized water several times until a neutral pH was obtained. The fabricated nanobelts were deposited into membranes or annealed at 700 °C for 1 h for experimental characterization. Commercially available TiO_2 P25 nanoparticles (Degussa, P25, specific area: 50.964 m^2/g) were used for comparison.

2.2. Membrane preparation

The TiO_2 nanobelt membranes were fabricated by a filtration and hot-press method [12]. Briefly, the TiO_2 nanobelt suspension was deposited on a Whatman® #1001042 paper filter within a vacuum filtration apparatus, with the deposited thick films subsequently sandwiched between two Al_2O_3 ceramic discs and pressed for 30 min at 200 °C by a uniaxial pressure machine exerting a force of 200 N. The resulting TiO_2 thick films were fired at 700 °C for 1 h to burn the filter paper away and shift the phase to more photocatalytic activated one (see Fig. S1† batch-processing of TiO_2 nanowire membranes).

2.3. Adsorption and photocatalytic degradation

The surface adsorption experiments were carried out by dispersing a slurry of prepared nanomaterials into 100 mL of 0.038 mM methylene blue solution (in ultrapure water, pH 6.8) in the dark at 22 °C with adsorption accelerated by magnetic stirring at 300 rpm. Photocatalytic degradation was assessed in the presence or absence of UV irradiation provided by a 100 W middle pressure mercury lamp (Cole Parmer) producing an intensity of 2.1 mW/cm^2 with the main emission wavelength of 365 nm positioned 5 cm from the surface of the solution. To saturate the surface adsorption capacity of the nanomaterials, each solution was first stirred in the dark for 1 h. To determine the active oxygen species, KI, isopropanol (i-PrOH) and catalase were used as quenchers during degradation analysis. The concentration of KI, i-PrOH, and catalase in the initial reaction solution were 0.1 mmol/L, 0.1 mmol/L and 500 mg/L according to previous studies [23,24].

2.4. Photocatalytic membrane reactor

A photocatalytic membrane reactor (PMR) was machined from stainless steel with two sealed chambers allowing for the secure insertion of a TiO_2 nanowire membrane between (see Fig. S2† Photocatalytic degradation experimental set-up: photocatalytic membrane reactor). A 3 mm thick quartz window was installed on the top surface of the PMR and sealed by an O-ring, with the TiO_2 membrane fixed parallel to the quartz window with a gap of 1 cm. Waterborne contaminants are introduced into the top chamber between the quartz window and TiO_2 membrane by an external peristaltic pump. After filtration the treated water was collected in the bottom chamber where it could be analyzed after a single pass (or recirculated for multiple passes) across the TiO_2 membrane. The TiO_2 membrane is underlain by a stainless steel mesh to avoid breakthrough from excessive pressure or flow; all water must pass through the membrane as it is sealed by a Teflon® O-ring on top and bottom surfaces. The recovery of TiO_2 membrane was tested by post-annealing at 250 °C for 10 min. After post-annealing, the adsorbed methylene blue was totally removed and membranes recovered into white. The annealed membrane was put back to the reactor and examined for reusability.

2.5. Characterization and analysis

The phase and microstructure of fabricated nanowires were examined by X-ray diffractometry, scanning electron microscopy (SEM) and transmission electron microscopy (TEM). TEM samples were prepared by suspension of TiO_2 nanobelts in ethanol and dripping into carbon Lacey film coated Cu grids. The specific surface area was determined by the Brunauer–Emmett–Teller (BET) method using N_2 adsorption data (Quantachrome Instruments NOVA 2200). X-ray photoelectron spectrum (XPS) measurements were carried out using a multi-technique ultra-high vacuum imaging XPS microprobe spectrometer (Thermo VG Scientific ESCALab 250) with a monochromatic *Al Kα* 1486.6 eV X-ray source. The spectrometer was calibrated by *Au* $4f_{7/2}$ (Binding energy of 84.0 eV) with respect to the Fermi level. The chamber vacuum level was maintained below 2×10^{-10} Torr. The constant pass energy was set at 160 eV for survey scans at 1 eV step. The pass energy of 20 eV was used for Na1s/K2p/Ti2p/O1s scans, with an energy resolution of 0.05 eV. Visual Raman spectra were measured using a Renishaw micro-Raman spectrometer with an Ar ion laser at an excitation wavelength of 488 nm. For both spectrometers the resolution was 1 cm^{-1}. The diffuse reflectance spectra were characterized by UV-NIR spectroscopy with an integrated spherical detector using $BaTiO_3$ as reference material. The methylene blue concentration was determined by adsorption at 663 nm.

3. Results and discussion

3.1. Phase identification and microstructural characterization

Fig. 1 shows typical SEM images of TiO_2 nanobelts grown (a) in 10 M NaOH solution for 72 h, (b) in 10 M KOH for 72 h and (c) in 10 NaOH solution for 48 h and then in 10 M KOH solution for 24 h. These experiments illustrate that NaOH solution is necessary for the formation of TiO_2 nanobelts with widths ranging from 30 to 100 nm, lengths in the range of tens of micrometers, but of pretty thin thickness. However, when KOH solutions alone are employed, the nanowires become even narrower, with widths shrinking to a few nanometers, but retaining lengths up to a few micrometers. Such variation in nanowire morphology arising from substitutions in alkaline solutions is consistent with previous studies [13]. However, nanowires grown in consecutive NaOH and KOH alkaline solutions displayed an innovative structure, in which 20–50 nm nanoparticles were synthesized on the surface of the nanobelts, with some connecting different nanobelts. These hierarchical structures form complex 3D networks differing from the entangled nanobelts that arise from growth in single alkaline solutions since these hierarchical nanobelts are joined or welded via the nanoparticles. It is evident that these hierarchical structures are not a simple mixture of nanobelts and nanoparticles since extended ultra-sonication treatment of suspension solution does not yield the separation of nanobelts and nanoparticles. X-ray diffraction patterns for nanowires grown in NaOH, KOH, or sequential NaOH/KOH solutions are shown in Fig. 2, and peaks can be indexed by the anatase phase for nanowires grown in NaOH (JCPDS 46-1238). For KOH solution the peaks are much wide with remarkable noise although the dominant phase is still anatase. In NaOH/KOH solution anatase peaks are slightly sharper than in KOH. This can be understood due to a small nanowire grown in KOH addition and hierarchic structures appeared in sequential solutions. Although the morphology of these nanowires differs dramatically, the dominant phase is the same after annealing at 700 °C. In order to further elucidate the chemical purity three kinds of TiO_2 nanowires are examined by X-ray Photoelectron Spectroscopy (XPS, shown in

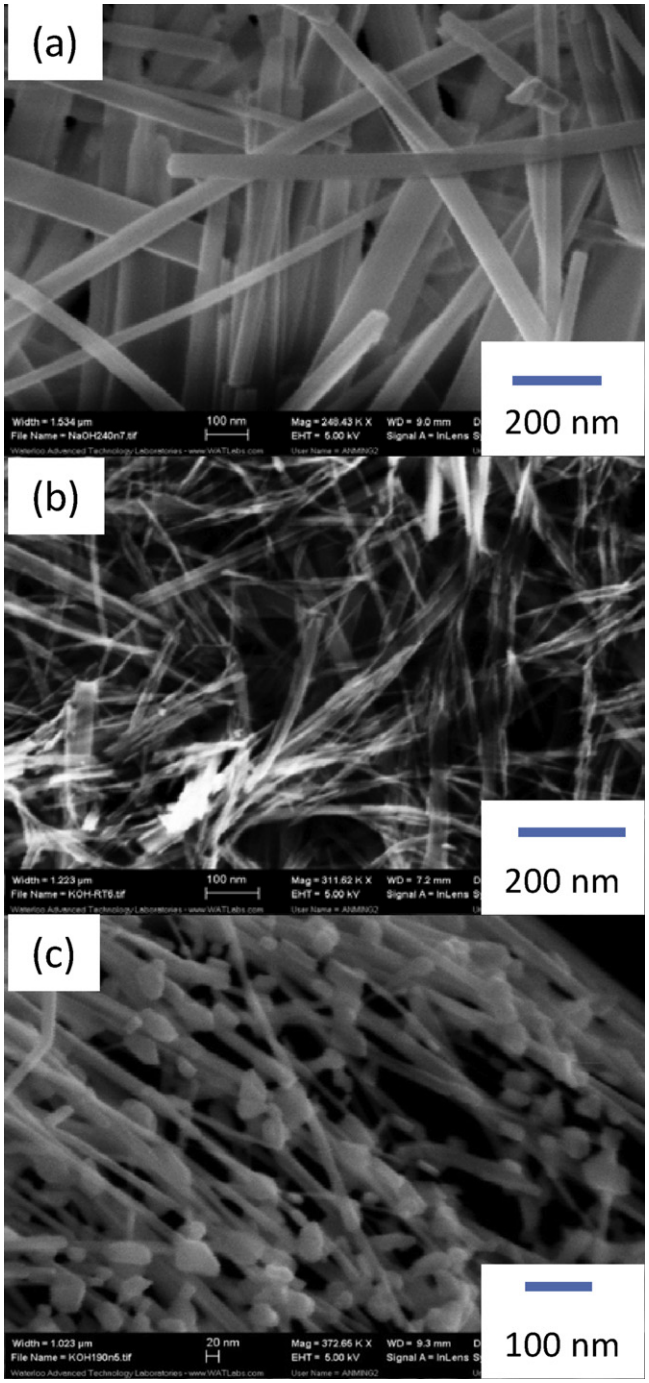

Fig. 1. Scanning electron microscopy images of TiO_2 nanobelts grown in (a) 10 M NaOH solution at 190 °C for 72 h, (b) in 10 M KOH at 190 °C for 72 h and (c) in 10 M NaOH at 190 °C for 48 h and then in 10 M KOH at 190 °C for 24 h.

Fig. 3). The survey unveils that Ti and O are the dominant compositions co-existing with minor C, Na and/or K. The Ti 2p3/2 and Ti 2p1/2 peaks can be identified at 464.3 eV and 458.5 eV, respectively, which are consistent with the typical values for TiO_2 [25,26]. The almost identical Ti2p doublet in all three compositions indicate that Ti keeps the similar tetravalent bonding state [26,27]. From the peak areas of C1s at 284.6 eV, Na1s at 1070.7 eV and K2p at 294.7 eV one can deduce their atomic percentages in the corresponding compositions. The concentration of C yields 6% for nanowires from NaOH solution, 5.2% from NaOH–KOH and 5% from KOH solution. The carbon is induced by carbonyl solvents added as an oxidizer during hydrothermal growth [11,22]. Na is founded as 3.7% and

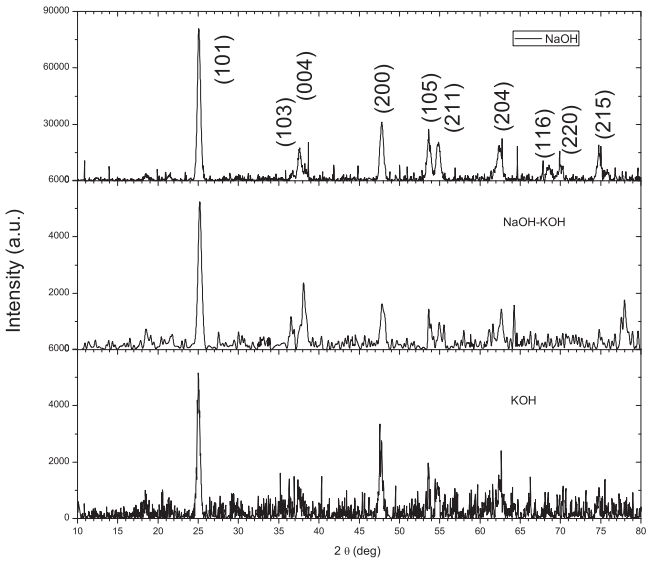

Fig. 2. X-ray diffractometry patterns of three TiO_2 nanomaterials: (a) nanobelts grown in NaOH solution, (b) nanobelts fabricated in KOH solution, and (c) hierarchical nanobelts grown sequentially in NaOH and KOH solutions.

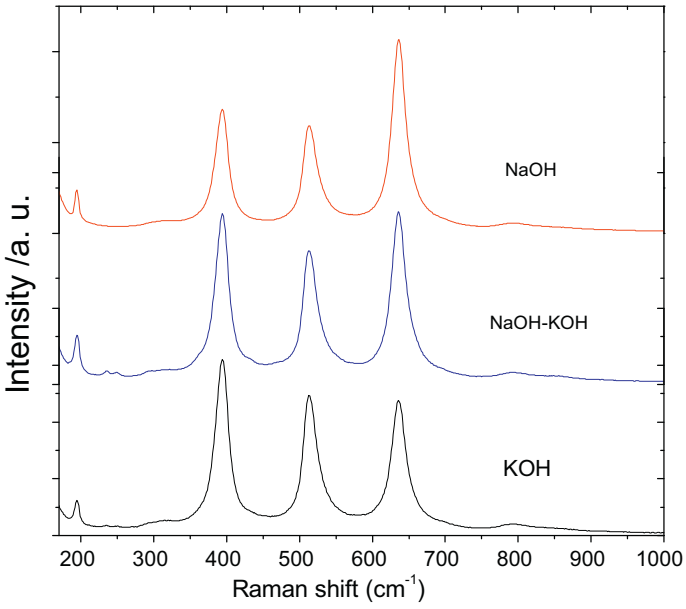

Fig. 4. Raman spectra of TiO_2 nanowires grown from three kinds of alkaline solutions. Excitation wavelength is 488 nm.

4.3% in nanowires separately grown in NaOH and NaOH–KOH solutions while the K fraction is founded at 0.9% and 2.4% in wires from NaOH–KOH and KOH solutions, respectively. Such low concentrations show that the ion exchange by diluted HCl is very effective to eliminate alkaline ions [28,29]. The high purity of TiO_2 nanowires can be also evident by Raman spectra. Fig. 4 shows the Raman spectra for three kinds of nanowires. Typical modes of TiO_2 anatase phase at 197, 399, 515, and 639 cm^{-1} can be clearly observed [26,28,30]. The low mode at 144 cm^{-1} is out of the effective range of device detection. The small peak at 247 cm^{-1} of nanowires grown in sequential solution could be relative to minor amorphous TiO_2 [31,32]. Therefore, three kinds of nanowires display similar Raman features. This indicates all of them are TiO_2 anatase although their morphologies are significantly different.

The diffuse reflection adsorption spectra demonstrate their energy gaps are around 3.0 eV for nanowires from NaOH solutions and 2.95 eV for nanowires either from NaOH–KOH or KOH solution (Fig. 5). It is important to point out that hierarchical nanobelt membranes (NaOH–KOH) display the enhanced absorbance (1.3 compared to 0.9 for NaOH and KOH nanowires) within UV wavelengths, confirming the unusual light absorption capacities of these novel structures. Such an absorption enhancement, which has been observed in a variety of hierarchical structures [33–35], arses from the multi-scattering of mesoporous structures [33–36]. The detailed lattice hierarchical structure of both surface TiO_2 nanoparticles and long nanobelts shown in Fig. 1(c) can be seen in the TEM images of Fig. 6. The lattice orientation can be attributed to the materials being in the anatase phase, which is in agreement with the XRD results. Fig. 6a shows two welded multi-layered nanobelts joined through shared layers. Surface nanoparticles may be attached at angles to the orientation of the core nanowires, sometimes separated by an amorphous layer between the oriented surface nanoparticles and underlying nanobelts (Fig. 6b). In

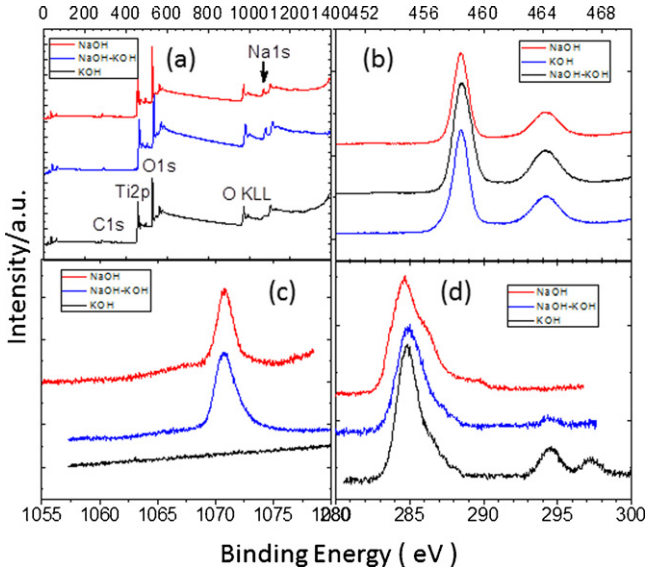

Fig. 3. X-ray Photoelectron spectra of three kinds of TiO_2 nanowires. (a) Survey scan. "In MNN" comes from Indium substrate. (b) Ti2p doublets. (c) Na1s peak and (d) C1s and K2p peaks.

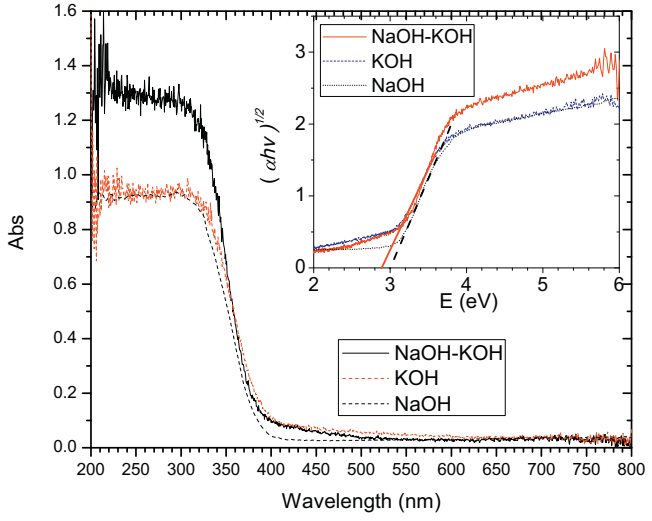

Fig. 5. UV-NIR diffuse reflection adsorption spectrum of TiO_2 nanobelt membranes measured by an integrated sphere detector. Inset is the analysis of optical gap by Tauc formula.

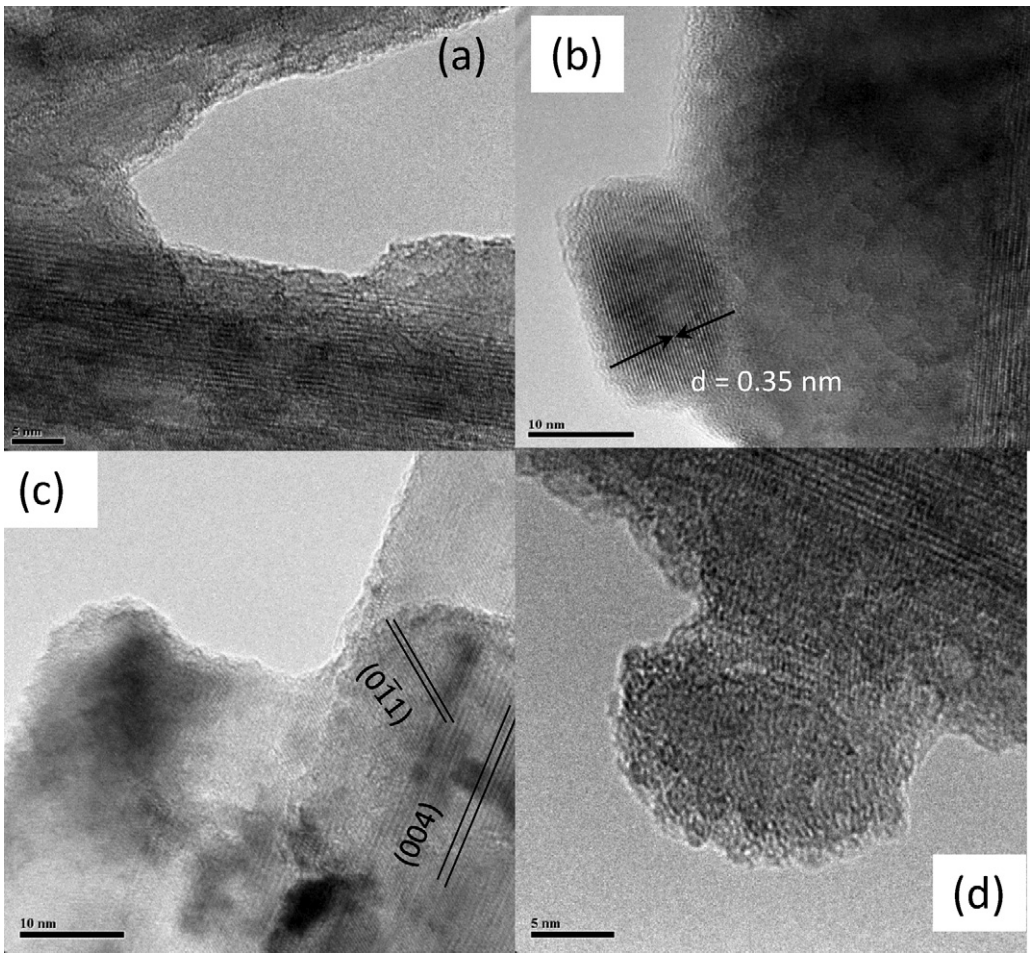

Fig. 6. TEM images of hierarchical TiO_2 nanobelts: (a) two joined nanobelts; (b) a nanoparticle adhered onto a nanobelt. Note the amorphous shell between crystalline core and surface nanoparticles. The lattice distance corresponds to (1 0 1) planes of anatase phase; (c) a crystalline nanoparticle orientated parallel to the nanobelt orientation; (d) an amorphous nanoparticle grown on the nanobelt.

some instances, the surface particles are almost perfectly aligned with the orientation of their basal nanobelts (Fig. 6c), while in others the surface nanoparticles themselves contain amorphous areas with little defined orientation as shown in Fig. 6(d). There appears to be no general relationship coordinating the orientation of surface nanoparticles and their basal nanobelts. Nevertheless, no sodium titanate or potassium titanate are evident in TEM observation in various nanowires [28,29,37]. This displays that TiO_2 anatase is the dominant composition in current nanowires with hierarchical structures, consistent with XRD and Raman data. The specific surface areas induced by the differing alkaline solutions are 16.709 m^2/g for anatase nanowires obtained from NaOH solution, 170.211 m^2/g for anatase nanowires autoclaved from KOH solution, and an enhanced specific surface area of 47.614 m^2/g for hierarchical nanobelts produced by sequential exposure to NaOH and KOH (Table 1).

To better understand the conditions favoring the growth of the current hierarchical structures, the use of sequential alkaline solutions was contrasted with results from mixtures of two alkaline solutions. The growth morphology of TiO_2 nanobelts with increasing KOH concentrations is provided in supplementary materials (see Fig. S3† TiO_2 nanowires growth with various KOH/NaOH ratios in solution), which demonstrates a similar hierarchical structure can be generated with a proper NaOH:KOH ratio of approximately 5:2. Higher ratios of KOH suppress both the nanobelt width and the mass of nanobelts obtained. This result is consistent with previous report [13], where TiO_2 nanobelts with a width of 20–100 nm are fabricated in a NaOH solution while narrow TiO_2 nanobelts of 10 nm in width are grown in a KOH solution. As nanobelt shape depends on different growth rates at variable planes, the present hierarchical structure of adhering nanoparticles on nanobelt surfaces are the net result of competing growth induced by the respective NaOH and KOH solutions [11,13]. It is notable that in the sequential growth, although there are only potassium ions in the 2nd growth stage the initial composite is $Na_2Ti_3O_7$ [11]. There are still a competitive crystalline favorite by Na and K ions, respectively.

Table 1
Characteristics of TiO_2 nanomaterials as adsorbents and photocatalysts. k_i is the intra-particle diffusion rate, and the i is relative to continuous diffusion stages correlated to the macro- and meso-pore structure of the adsorbent. K_{ap} is the apparent reaction rate in photocatalyic degradation according to pseudo-first model.

Nanomaterials	S (m^2/g, BET)	q_e (mg/g)	K_1 (mg/g $min^{0.5}$)	K_2 (mg/g $min^{0.5}$)	K_{ap} (min^{-1})
P25	50.236	65.2	8.1	4.5	0.045
NaOH	16.709	88.6	12.7	2.8	0.057
KOH	170.211	170	30.4	0.56	0.021
NaOH–KOH	47.614	159	26.7	2.8	0.089

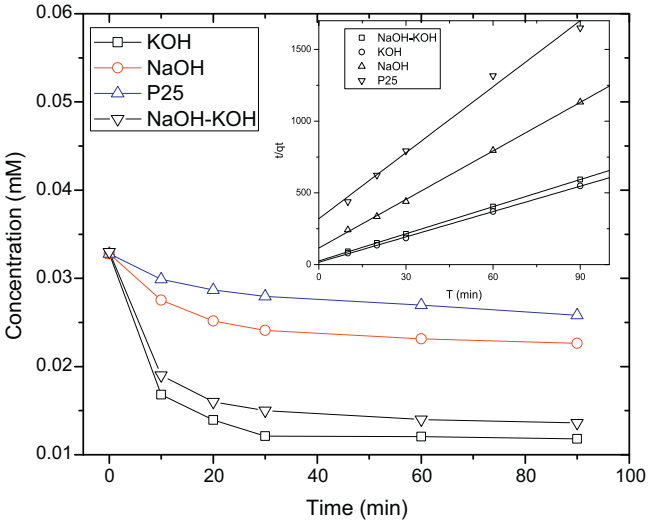

Fig. 7. Adsorption kinetics of methylene blue onto 4 TiO_2 nanomaterials: P25 and three nanobelts autoclaved from NaOH, KOH and sequential NaOH–KOH solutions, respectively. The solution volume is 100 mL, pH 6.8. Inset: the time profile fitted to pseudo-second order kinetics. The obtained equilibrium adsorption capacity, q_e, is provided in Table 1.

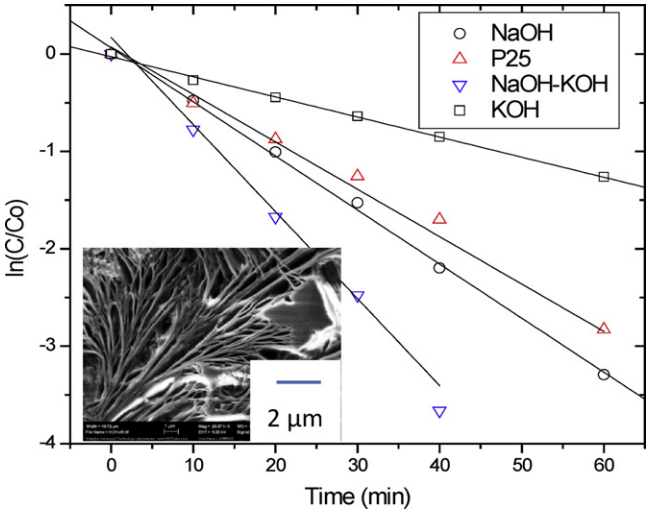

Fig. 8. Kinetic analysis of rates of degradation by photocatalysis with four kinds of TiO_2 catalysts. The solid lines fit the pseudo first-order model. The apparent degradation rate is given in Table 1. Inset: SEM images TiO_2 nanowires synthesized in KOH solution. SEM samples are fabricated by drying the aquatic suspension of TiO_2 nanowires.

3.2. Chemical adsorption

The adsorption kinetics of methylene blue in the presence of four different TiO_2 nanomaterials at room temperature is demonstrated in Fig. 7. While the adsorption capacity of the nanowires were high (especially those grown in KOH or NaOH/KOH owing to their large specific surface areas), the commercial P25 nanoparticles displayed a low adsorption rate, despite their fairly high specific surface area of 50.694 m^2/g. While specific surface area is important, adsorption is also dependent on the surface charge of the nanoparticle/nanowire, the adsorbent mass, ambient pH values and the temperature of the solution. For all TiO_2 nanomaterials, adsorptive capacity is nearly saturated after 30 min, but notably, the NaOH–KOH hierarchical nanobelts display enhanced adsorption capacities compared to smooth TiO_2 nanowires grown from NaOH solution.

With respect to kinetic modeling, the pseudo-second-order model has been evaluated to reveal the adsorption mechanism, $t/q_t = 1/(kq_e^2) + t/q_e$ where $q_t = (C_0 - C_t)(v/w)$ is the mass of methylene blue adsorbed (g/g) at time t by 1 g of hierarchical nanobelts, C_0 and C_t are the initial concentration and concentration at time, t, v is the volume of the solution, and w is the mass of the adsorbent used, q_e is the equilibrium adsorption capacity, and k is the rate constant of pseudo-second-order adsorption [38]. The linear fit (inset on Fig. 7) indicates that the adsorption mechanism is based on chemisorption since the pseudo-second order model is based on a chemical reaction between dimeric dye micelles and sorbent [39,40]. Application of best fit determined the equilibrium adsorption capacities of P25 nanoparticles and TiO_2 nanowires autoclaved in NaOH, KOH, NaOH–KOH as 65.2, 88.6, 170 and 159 mg/g, respectively. The adsorption capacities of KOH and NaOH–KOH nanobelts approach those of commercial activated carbon (200–400 mg/g [41]) and titanate nanowires (196 mg/g) [9]. This shows a possibility to using the chemical adsorption of these nanowire membranes to remove the micro-pollutants during water treatment.

To optimize the TiO_2 nanowire membrane microstructure for adsorption, it is necessary from a mechanistic viewpoint, to identify the steps involved in adsorption. It is well known that adsorption incorporates external mass transfer and intra-particle diffusion [38,42]. Intra-particle diffusion, which can be described by Weber and Morris' model, $q_t = k_i t^{1/2} + c$ where c is the constant and k_i is the intra-particle diffusion rate [43], may be further separated into a few continuous diffusion stages correlated to the macro-, meso- and micropore structure of the adsorbent [42,44]. The plotting of q_t as a function of $t^{1/2}$ reveals two linear ranges in the curve reflecting the transition from adsorption to one kind of pore to another (see Fig. S4† Analysis with Weber and Morris' model). The slope of the linear relationship, k_i, characterizes the rate of intra-particle diffusion; the value of k_i given by the best fit is shown in Table 1. It is obvious that for the three nanobelts, k_i has two different values while P25 displays similar values over two diffusion regimes. These results are consistent with the adsorption reported for sphagnum peat [44], where the continuous branching pore distribution was proposed. It is reasonable to deduce that a similar pore distribution is evident within the current membranes. However, modified peat amended with polyvinylalcohol and formaldehyde displayed a mitigated variation in pore size [39], similar to that of P25. It seems indicating that the chemical adsorption is not a simple surface adsorption. The further discrimination of different adsorption mechanics is interesting but beyond the scope of this study.

3.3. Photocatalytic degradation

Photocatalytic degradation of methylene blue in the presence of various TiO_2 nanomaterial suspensions is illustrated in Fig. 8. Although nanobelts produced from KOH possess strong surface adsorption properties, these nanomaterials only weakly photodegraded methylene blue molecules, displaying similar properties to those of titanate nanotubes [11]. Nanobelts from NaOH are slightly more effective at photocatalytically degrading methylene blue than P25, while hierarchical TiO_2 nanobelts autoclaved from NaOH–KOH solution display the strongest degradation. Photocatalytic degradation can be described by pseudo first-order kinetics: $-dC/dt = K_{ap}C$, where the C is the concentration and K_{ap} is the apparent reaction rate. A time function $ln(C_0/C) = K_{ap}t$ can be deduced by integrating the above equation where C_0 is the initial concentration. The linear relationship in Fig. 8 is the best fit to the pseudo first order model, yielding the value of K_{ap} as 0.021, 0.045, 0.057 and 0.089 min^{-1} for nanobelts from KOH, P25, NaOH and NaOH–KOH, respectively. These degradation rates are better than that of hierarchical TiO_2 nanoflakes [35] and hollow TiO_2 anatase microspheres

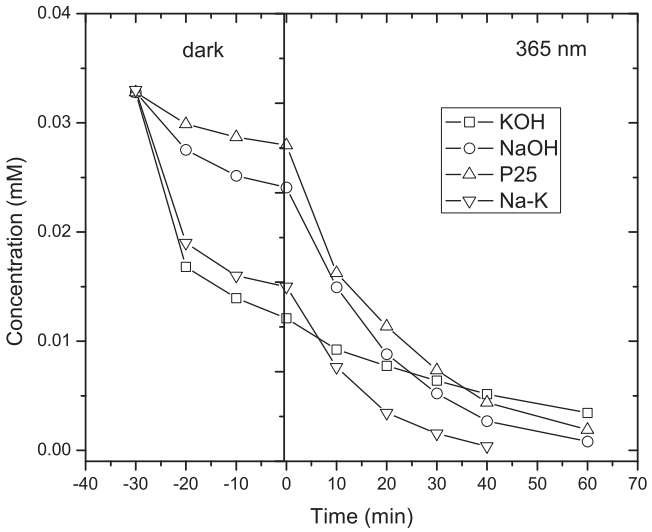

Fig. 9. Adsorption and photocatalytic removal of methylene blue by a TiO_2 nanomaterials suspended as a slurry. The dark regime illustrates removal by adsorption over 30 min while the 365 nm UV regime illustrates photocatalyic degradation.

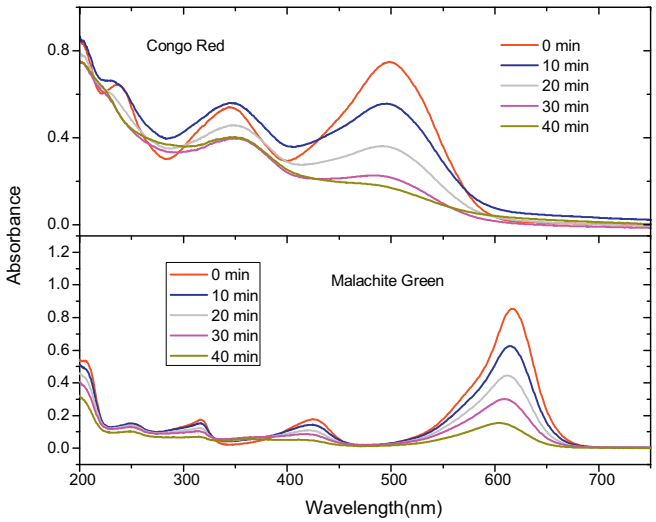

Fig. 10. Photocatalytic degradation of Malachite green and Congo red solutions with hierarchic TiO_2 nanowires exposing to 365 nm UV light.

with more reactive (0 0 1) facets as photocatalysts [45]. The performance of current hierarchical TiO_2 nanowires can be compared to nanoheterostructure Ag/TiO_2 nanowires [17], where the concentration of methyl orange is degraded in 2 orders within 30 min. Nevertheless, the photocatalytic performance is determined by various factors, as mentioned in the introduction. Shown in the inset to Fig. 8, we find that nanowires from KOH solution tend to aggregate in aquatic media and forms secondary micro-sized bundles. It has been shown that an aggregated semiconducting catalyst results in a lower photocatalytic capacity [46]. The synergistic decoloration of methylene blue by both surface adsorption and photocatalytic degradation under 365 nm UV illumination is shown in Fig. 9. It is notable that the chemical adsorption and degradation are two separated color removal mechanisms. Nanowires from KOH solutions possess a superior surface adsorption while their photocatalytic degradation mechanism is relatively weak. While nanowires from NaOH have an improved degradation performance their chemical adsorption capacity is limited. The chemical adsorption is correlated with the specific surface area (see Table 1). In general, hierarchical nanobelts generated with NaOH/KOH alkaline solutions demonstrate a significant improvement in color removal by combining two mechanisms. This is an attractive feature of current hierarchical nanobelts. Shown in Fig. 10, two typical dyes, Malachite green and Congo red are chosen for examine the extensive effectiveness of hierarchical nanowires. Both concentrations can be dramatically degraded with exposing to 365 nm UV light with one hour. The analysis shows both of them follow a pseudo-first order model with degradation rates of 0.057/min for Malachite green and 0.034/min for Congo red.

3.4. Identification of reaction oxygen species

The active oxygen species have been extensively investigated with commercial P25 TiO_2 nanoparticles and TiO_2 coated nonwoven paper [23,24], where hydroxyl, positive holes and hydrogen peroxide are identified as dominant oxygen species. In this experiment, we employ the similar techniques to identify the presence and roles of these species. Shown in Fig. 11, degradation rates with adding three kinds of specie quenchers are examined. Isopropanol is used to scavenge $OH^{\bullet}$, KI can remove valence band holes and $OH^{\bullet}$ radicals while catalase is a quencher of H_2O_2 [23,47]. Therefore, 60.4% decrease of k due to i-PrOH can be attributed to the removal of $OH^{\bullet}$. Furthermore, it can deduce that 21.6% of degradation is based on valence band holes from an 82% decrease of the degradation rate due to KI addition. The scavenging experiment with catalase shows the significant role of H_2O_2 during dye degradation. There are two origins to generate H_2O_2, either from TiO_2 photocatalysis or dye direct photolysis [23,24]. The removal H_2O_2 results in 52.3% of decrease of K. However, H_2O_2 does not directly oxidize MB rather works as intermediate species to generate $OH^{\bullet}$. Since both H_2O_2 and holes can form $OH^{\bullet}$, we can deduce about the hole contribution due to photolysis is 8.1%. This value is obtained by subtracting 52.3% from 60.4%. One can easily figure out the total hole contribution for dye degradation is 29.7% by adding 8.1% to 21.6%. Hence, the left 9.9% can be attributed to the mixture effect of secondary species, such as, $O_2^{\bullet-}$, $HO_2^{\bullet-}$ and O_3. The obtained degradation fractions, 60.4% from $OH^{\bullet}$, 29.7% from holes and 9.9% from other oxidative species are approximately consistent with the previous report with P25 nanoparticles [24], where the values are 62.3%, 31.1% and 6.6%, respectively.

The mechanism by which hierarchical structures enhance photocatalytic efficiency might be insightful for expropriating these properties in additional applications. Initially, hierarchical

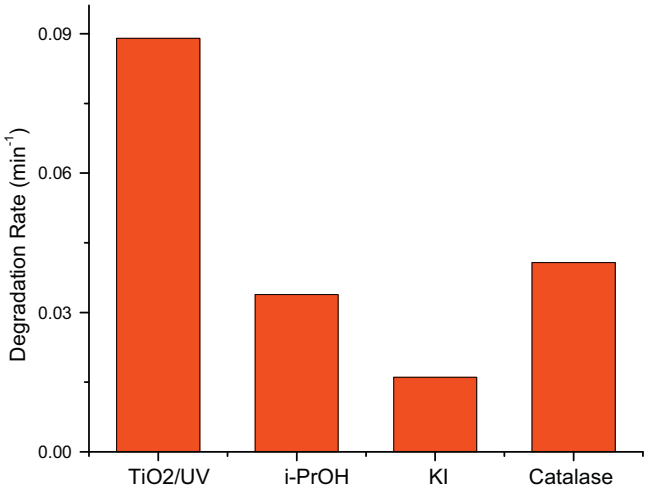

Fig. 11. Degradation rates of methylene blue with hierarchical TiO_2 nanowires with oxygen species quenchers: isopropanol, KI and catalase.

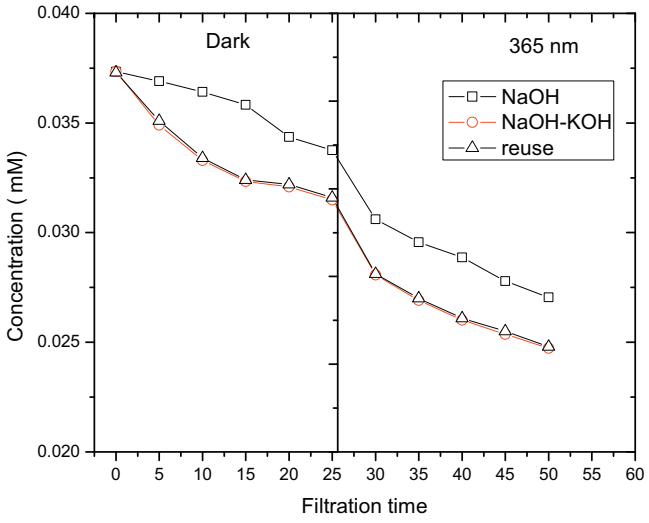

Fig. 12. Synergistic (adsorption/photocatalytic degradation) decoloration of methylene blue by TiO_2 nanobelt membranes in a prototype photocatalytic membrane reactor. The filtration flow rate was 50 mL/min with the dark regime corresponding to the surface adsorption and the 365 nm UV regime illustrating the combined effects of surface adsorption and UV photocatalytic degradation. Two nanomembranes membranes are compared: membranes autoclaved in NaOH solution alone, and hierarchical nanobelt membranes sequentially autoclaved in NaOH and KOH. The reuse curve displays the performance of TiO_2 nanobelt membranes after 3 continuing experimental cycles. Each cycle includes 5 continuing adsorptions in dark and then 5 continuing degradations under UV. After each cycle, the membrane is recovered by annealing at 250 °C for 10 min.

structures exhibit heightened UV light adsorption due to their complicated surface which can enhance light harvesting to improve photocatalytic efficiency (Fig. 5). As both $OH^{\bullet}$ and holes are very transient species (half-life $\sim 10^{-9}$ s), photocatalytic degradation is limited to the vicinity of the nanomaterial surface, reinforcing the importance of surface adsorption behavior by the nanomaterial. Hierarchical nanobelts displayed enhanced surface adsorption properties, which are beneficial for degrading methylene blue molecules in the vicinity of the nanobelts. Finally, hierarchical structures may also facilitate the separation of electron–hole pairs by a charge-transfer mechanism between crystalline nanobelts and amorphous surfaces similar to surface modification by vitamin C [41]. The amorphous surface area can trap charge carriers, thereby reducing the recombination of electron–hole pairs, which may account for the enhanced photocatalytic efficiency of hierarchical nanobelts relative to those derived from NaOH alone. However, elucidating the underlying mechanism behind this photocatalytic enhancement is beyond the scope of the current work.

3.5. *Prototype TiO_2 nanowire membrane reactors*

We further characterized the decoloration of methylene blue by TiO_2 nanobelt membranes in the prototype photocatalytic membrane reactor using NaOH and NaOH/KOH derived membranes in the presence and absence of UV (Fig. 12). Notably, hierarchical nanobelts demonstrate both enhanced surface adsorption and photocatalytic degradation relative to TiO_2 nanobelts autoclaved from NaOH solution alone. However, when using hierarchical membranes mounted in the PMR, both the adsorption and degradation rates dramatically decreased relative to the use of nanobelt slurry in solution. The decline in surface adsorption can be attributed to the significant reduction of contact area between the waterborne dye and membranes since only the top membrane surface is exposed to the dye. Similarly, the lower photocatalytic degradation rate is also a function of the limited upper membrane surface area being exposed to UV light. Enlarging the illumination area should be considered to optimize the membrane performance. Nevertheless, the preliminary experiments with the PMR demonstrate successful methylene blue removal by adsorption and photocatalytic degradation. Since the present membranes we utilized in the PMR can also filter nanowires, it would be possible to combine the use of these nanomaterials in a slurry configuration with their filtration by the same material configured into a membrane in the PMR to enhance water treatment. Under this scenario, adsorption, photocatalytic degradation and nanocatalyst separation could be realized in the same PMR.

After filtration the color of TiO_2 nanobelt membranes turned from white to blue due to the surface adsorbed methylene blue. The recovery of TiO_2 nanobelt membranes is tested by annealing the membrane at 250 °C for 10 min. Such a post-annealing can effectively remove the adsorbed dye. The membrane is reused to examine the reusability of membranes. Shown in Fig. 12, the membrane displays almost similar adsorption in the dark and photocatalytic degradation performance with 365 nm excitation for 4 repeated experimental cycles (for clearance only the data for the last repeated experimental cycle are shown). Each cycle includes 5 times of continuing adsorption followed by 5 times of continuing photocatalytic degradation. After each experimental cycle, the TiO_2 nanobelt membrane is recovered by annealing. Thus, the current experiment displays an excellent stability and recovery of TiO_2 nanobelt membranes.

Currently, up to 10 pieces of membranes with a mass of 0.2 g can be fabricated from one-pot synthesis (2 g, Fig. S1† batch-processing of TiO_2 nanowire membranes) while one furnace can simultaneously process 6–8 high pressure reactors in parallel. Consequently, over 50 individual membranes can be produced with one furnace, dramatically reducing fabrication costs. Compared to other methods to generate hierarchical structures, where either specific synthesis facility is required [35] or a complicated acidic post-treatment is employed [13], the current method presents a practical and simple protocol to fabricate hierarchical nanobelts scalable to a large mass production with superior photocatalytic degradation and surface adsorption performance. The current PMR can be easily modified to combine a compound parabolic solar collector for economical solar disinfection of water [1,48], potentially broadening application of these materials to water treatment scenarios within remote locations or developing countries.

4. Conclusions

Hierarchical TiO_2 nanobelts with surface TiO_2 nanoparticles have been synthesized by sequentially autoclaving in 10 M NaOH and 10 M KOH solutions at 190 °C. The resultant hierarchical nanomaterials displayed enhanced chemical adsorption and photocatalytic degradation properties towards the model dye methylene blue. The chemical adsorption of methylene blue followed a pseudo-second order kinetic degradation displaying rate-limited diffusion dependent on pore structure and size distribution. The dominant oxidative species were identified as hydroxyl radicals and valence band holes. In a prototype photocatalytic membrane reactor, adsorption, filtration and photocatalytic degradation can be combined to generate synergies in the decoloration of methylene blue. The present results demonstrate the proof-in-concept application of hierarchical TiO_2 nanobelt membranes for contaminant removal during water treatment.

Acknowledgements

This work has been financially supported by the Natural Sciences and Engineering Research Council of Canada through a strategic project grant, the Canadian Water Network Innovative

Technologies for Water Treatment Program, and the Canada Research Chairs Program. Technical support from Trojan UV, the City of Guelph Wastewater Services, Deep Blue NRG, and GE Water & Process Technologies are highly appreciated. X. Zhang would like to thank the Ontario Ministry of Research & Innovation and the Canadian Institutes of Health Research for financial supports.

Appendix A. Supplementary data

Supplementary data associated with this article can be found, in the online version, at http://dx.doi.org/10.1016/j.jphotochem.2013.01.015.

References

[1] S. Malato, J. Blanco, A. Vidal, C. Richter, Photocatalysis with solar energy at a pilot-plant scale: an overview, Applied Catalysis B 37 (2002) 1–15.
[2] C.D. Metcalfe, B.G. Koenig, D.T. Bennie, M. Servos, T.A. Ternes, R. Hirsch, Occurrence of neutral and acidic drugs in effluents of Canadian sewage treatment plants, Environmental Toxicology and Chemistry 22 (2003) 2872–2880.
[3] M.N. Chong, B. Jin, C.W.K. Chow, C. Saint, Recent developments in photocatalytic water treatment technology: a review, Water Research 44 (2010) 2997–3927.
[4] S. Malato, P. Fernandez-Ibanez, M. Maldonado, I.M. Blanco, W. Gernjak, Decontamination and disinfection of water by solar photocatalysis: recent review and trends, Catalysis Today 147 (2009) 1–59.
[5] L. Bousselmi, S.U. Geissen, H. Schroeder, Textile wastewater treatment and reuse by solar catalysis: results from a pilot plant in Tunisia, Water Science and Technology 49 (2004) 331–337.
[6] S. Mozia, M. Tomaszewska, A.W. Morawski, Photocatalytic membrane reactor (PMR) coupling photocatalysis and membrane distillation-effectiveness of removal of three azo dyes from water, Catalysis Today 129 (2007) 3–8.
[7] L. Rizzo, S. Meric, M. Guida, D. Kassinos, V. Belgiorno, Heterogeneous photocatalytic degradation kinetics and detoxification of an urban wastewater treatment plant effluent contaminated with pharmaceuticals, Water Research 43 (2009) 4070–4078.
[8] M. Rafaltullah, O. Sulaiman, R. Hashim, A. Ahmad, Adsorption of methylene blue on low-cost adsorbents: a review, Journal of Hazardous Materials 177 (2010) 70–80.
[9] K. Hu, X. Xiao, X. Cao, R. Hao, X. Zuo, X. Zhang, J. Nan, Adsorptive separation and photocatalytic degradation of methylene blue dye on titanate nanotube powders prepared by hydrothermal process using metal Ti particles as a precursor, Journal of Hazardous Materials 192 (2011) 515–520.
[10] V. Augugliaro, M. Litter, L. Palmisano, J. Soria, The combination of heterogeneous photocatalysis with chemical and physical operations: a tool for improving the photoprocess performance, Journal of Photochemistry and Photobiology C 7 (2006) 127–144.
[11] A. Hu, X. Zhang, K.D. Oakes, P. Peng, Y. Zhou, M. Servos, Hydrothermal growth of free standing TiO_2 nanowire membranes for photocatalytic degradation of pharmaceuticals, Journal of Hazardous Materials 189 (2011) 278–285.
[12] N. Barka, S. Qourzal, A. Assabbane, A. Nounah, Y. Ait-Ichou, Factors influencing the photocatalytic degradation of Rhodamine B by TiO2-coated non-woven paper, Journal of Photochemistry and Photobiology A 195 (2008) 346–351.
[13] X. Zhang, J. Pan, A. Du, W. Fu, D. Sun, J. Leckie, Combination of one-dimensional TiO_2 nanowire photocatalytic oxidation with microfiltration for water treatment, Water Research 43 (2009) 1179–1186.
[14] S.P. Albu, A. Ghicov, J.M. Macak, R. Hahn, P. Schmuki, Self-organized, free-standing TiO_2 nanotube membrane for flow through photocatalytic application, Nano Letters 7 (2007) 1286–1289.
[15] H.G. Yang, C.H. Sun, S.Z. Qiao, J. Zou, G. Liu, S.C. Smith, H.M. Cheng, G.Q. Lu, Anatase TiO_2 single crystals with a large percentage of reactive facets, Nature 453 (2008) 638–641.
[16] M. Liu, L. Piao, W. Lu, S. Ju, L. Zhao, C. Zhou, H. Li, W. Wang, Flower-like TiO_2 nanostructures with exposed {0 0 1} facets: facile synthesis and enhanced photocatalysis, Nanoscale 2 (2010) 1115–1117.
[17] W. Zhou, G. Du, P. Hu, G. Li, D. Wang, H. Liu, J. Wang, R. Boughton, D. Liu, H. Jiang, Nanoheterostructures on TiO_2 nanobelts achieved by acid hydrothermal method with enhanced photocatalyic and gas sensitive performance, Journal of Materials Chemistry 21 (2011) 7937–7945.
[18] Z. Zheng, H. Liu, J. Ye, J. Zhao, E.R. Waclawik, H. Zhu, Structure and contribution to photocatalytic activity of the interfaces in nanofibers with mixed anatase and TiO_2 (B) phases, Journal of Molecular Catalysis A 316 (2010) 75–82.
[19] D. Yang, H. Liu, Z. Zheng, Y. Yuan, J. Zhao, E. Waclawik, X. Ke, H. Zhu, An efficient photocatalyst structure: TiO_2 (B) nanofibers with a shell of anatase nanocrystals, Journal of the American Chemical Society 131 (2009) 17885–17893.
[20] P. Fu, P.Y. Zhang, Uniform dispersion of Au nanoparticles on TiO_2 film via electronstatic self-assembly for photocatalytic degradation of bisphenol A, Applied Catalysis B 96 (2010) 176–184.
[21] Z. Liu, X. Zhang, S. Nishimoto, M. Jin, D.A. Tryk, T. Murakam, A. Fujishima, Anatase TiO_2 nanoparticles on rutile TiO_2 nanorods: a heterogeneous nanostructure via layer-by-layer assembly, Langmuir 23 (2007) 10916–10919.
[22] A. Hu, X. Zhang, D. Luong, K.D. Oakes, M.R. Servos, R. Liang, S. Kurdi, P. Peng, Y. Zhou, Adsorption and photocatalytic degradation kinetics of pharmaceuticals by TiO_2 nanowires during water treatment, Waste Biomass Valorization 3 (2012) 443–449.
[23] X. Zhang, T. Zhang, J. Ng, D. Sun, High-performance multifunctional TiO_2 nanowire ultrafiltration membrane with a hierarchical layer structure for water treatment, Advanced Functional Materials 19 (2009) 3731–3736.
[24] X. Zhang, D.D. Sun, G. Li, Y. Wang, Investigation of the roles of active oxygen species in photodegradation of azo dye AO7 in TiO_2 photocatalysis illuminated by microwave electrodeless lamp, Journal of Photochemistry and Photobiology A 199 (2008) 311–315.
[25] G. Wang, H. Wang, Y. Ling, Y. Tang, X. Yang, R.C. Fitzmorris, C. Wang, J.Z. Zhang, Y. Li, Hydrogen-treated TiO_2 nanowire arrays for photoelectrochemical water splitting, Nano Letters 11 (2011) 3026–3033.
[26] X. Chen, L. Liu, P.Y. Yu, S.S. Mao, Increasing solar absorption for photocatalysis with black hydrogenated titanium dioxide nanocrystals, Science 331 (2011) 746–750.
[27] A. Foli, I. Pochard, A. Nonat, U.H. Jackbsen, A.M. Shepherd, D.E. Macphee, Engineering photocatalytic cements: understanding TiO_2 surface chemistry to control and modulate photocatalytic performances, Journal of the American Ceramic Society 93 (2010) 3360–3369.
[28] R.A. Zarate, S. Fuentes, J.P. Wiff, V.M. Fuenzalida, A.L. Cabrera, Chemical composition and phase identification of sodium titanate nanostructures grown from titania by hydrothermal processing, Journal of Physics and Chemistry of Solids 68 (2007) 628–637.
[29] Q. Chen, W. Zhou, G. Du, L.M. Peng, Trititanate nanotubes made via a single alkali treatment, Advanced Materials 14 (2002) 1208–1211.
[30] L.C. Sikuvhihulu, N.J. Coville, T. Ntho, M.S. Scurrell, Potassium titanate: an alternative support for gold catalysed carbon monoxide oxidation? Catalysis Letters 123 (2008) 193–197.
[31] Q. Li, B. Liu, L. Wang, D. Li, R. Liu, B. Zou, T. Cui, G. Zou, Pressure-induced amorphization and polyamorphism in one-dimensional single crystal TiO_2 nanomaterials, Journal of Physical Chemistry Letters 1 (2010) 309–314.
[32] T. Mazza, E. Barborini, P. Piseri, P. Milani, D. Cattaneo, A. Li Bassi, C.E. Bottani, C. Ducati, Raman spectroscopy characterization of TiO_2 rutile nanocrystals, Physical Review B 75 (2007), 045416-1-5.
[33] Z. Zhang, P. Wang, Optimization of photoelectrochemical water splitting performance on hierarchical TiO_2 nanotube arrays, Energy and Environmental Science 5 (2012) 6506–6512.
[34] W. Yang, F. Wan, Q. Chen, J. Li, D. Xu, Controlling synthesis of well-crystallized mesoporous TiO_2 microspheres with ultrahigh surface area for high-performance dye-sensitized solar cells, Journal of Materials Chemistry 20 (2010) 2870–2876.
[35] Y. Tang, P. Wee, Y. Lai, X. Wang, D. Gong, P.D. Kanhere, T. Lim, Z. Dong, Z. Chen, Hierarchical TiO_2 nanoflakes and nanoparticles hybrid structure for improved photocatalytic activity, Journal of Physical Chemistry C 116 (2012) 2772–2780.
[36] A. Usami, Theoretical study of application of multiple scattering of light to a dye-sensitized nanocrystalline photoelectrochemical cell, Chemical Physics Letters 277 (1997) 105–108.
[37] X. Meng, D. Wang, J. Liu, S. Zhang, Preparation and characterization of sodium titanate nanowires from brookite nanocrystallites, Materials Research Bulletin 39 (2004) 2163–2170.
[38] Q. Sun, L. Yang, The adsorption of basic dyes from aqueous solution on modified peat–resin particles, Water Research 37 (2003) 1535–1544.
[39] K. Vasanth Kumar, V. Ramamurthi, S. Sivanesan, Modeling the mechanism involved during the sorption of methylene blue onto fly ash, Journal of Colloid and Interface Science 284 (2005) 14–21.
[40] Y. Ho, G. McKey, The kinetics of sorption of basic dyes from aqueous solution by sphagnum moss peat, Canadian Journal of Chemical Engineering 76 (1998) 822–827.
[41] T. Rajh, J.M. Nedeljkovic, L.X. Chen, O. Poluektov, M.C. Thurnauer, Improving optical and charge separation properties of nanocrystalline TiO_2 by surface modification with vitamin C, Journal of Physical Chemistry B 103 (1999) 3515–3519.
[42] G.M. Walker, L. Hansen, J.A. Hanna, S.J. Allen, Kinetics of a reactive dye adsorption onto dolomitic sorbents, Water Research 37 (2003) 2081–2089.
[43] W.J. Weder, J.C. Morris, Kinetics of adsorption on carbon from solution, Journal of the Sanitary Engineering Division ASCE 89 (1963) 31–60.
[44] S.J. Allen, G. Mckay, K.Y.H. Khader, Intraparticle diffusion of a basic dye during adsorption onto sphagnum peat, Environmental Pollution 56 (1989) 39–50.
[45] S. Liu, J. Yu, M. Jaroniec, Tunable photocatalytic selectivity of hollow TiO_2 microsphere composed of anatase polyhedral with exposed {0 0 1} facets, Journal of the American Chemical Society 132 (2010) 11914–11916.
[46] A. Mills, S.L. Hunte, An overreview of semiconductor photocatalysis, Journal of Photochemistry and Photobiology A 108 (1997) 1–35.
[47] K. Ishibashi, A. Fujishima, T. Watanabe, K. Hashimoto, Quantum yields of active oxidative species formed on TiO_2 photocatalyst, Journal of Photochemistry and Photobiology A 134 (2000) 139–142.
[48] J. Blanco, S. Malato, P. Fernandez, A. Vidal, A. Morales, P. Trincado, J.C. Oliveira, C. Minero, M. Musci M., C. Casalle C., M. Brunotte, S. Tratzky, N. Dischinger, K.H. Funken, C. Sattler, M. Vincent, M. Collares-Pereira, J.F. Mendes, C.M. Rangel, Compound parabolic concentrator technology development to commercial solar detoxification applications, Solar Energy 67 (1999) 317–330.